18th AIAA/CEAS Aeroacoustics Conference (33rd AIAA Aeroacoustics Conference)
04 - 06 June 2012, Colorado Springs, CO

AIAA 2012-2099

On Detrimental Effects of Excrescences on the Slat Noise

Lukas Bandle*
Universität Stuttgart, Stuttgart, Baden-Württemberg, Germany

Daniel S. Souza†
Universidade de São Paulo, São Carlos, São Paulo, Brazil

Leandro G. C. Simões‡
Embraer, São José dos Campos, São Paulo, Brazil

Marcello A. F. Medeiros §
Universidade de São Paulo, São Carlos, São Paulo, Brazil

In airplane landing the slat noise is already a barrier to the development of quieter commercial airplanes. Investigations have been made by several research groups to understand the mechanism of noise generation in slat and develop better tools to predict it. Most of the published works related to slat noise considers clean idealized geometries, whereas real slats contain some imperfections to enable its operation. The influence of a protrusion on the slat cavity surface on the unsteady flow around the slat and on the propagated sound was here investigated via numerical calculation. The protrusion was a sealing device to avoid metal-metal contact. Lattice-Boltzmann method was used in the computations. The effect of the seal on the mean surface pressure distribution is limited to the region close to it. When the seal is positioned inside the recirculation zone, the region next to the cusp present less fluctuation intensity and the vortices formed in the mixing layer keep two-dimesionality for a longer distance in the way to the reattachment point. The noise propagated to far-field also present more intense low frequency tonal peaks. Although discretization as fine was $0.15mm$ was employed, fluctuations of a specific frequency band were still mesh dependent.

Nomenclature

s	Distance to slat trailing edge
s_{rp}	s of slat reattachment point
h	Seal height
c	Stowed chord
c_s	Slat chord
M	Mach number
U_∞	Flow inlet velocity
f	Probability density function
f^{eq}	Equilibrium probability density function
$\vec{c}$	Particle velocity
S_{max}	Total distance from cusp to reattachment
S	Distance from cusp along the mixing layer
St	Strouhal number
y^+	Dimensionless wall distance yu_τ/ν_o

Greek:

δ_{TE}	Slat trailing edge thickness
τ	relaxation time

*Uni-Stuttgart, IAG, Stuttgart, Germany. Lukas-Bandle@gmx.de
†USP, SEA, São Carlos, Brazil. dss-em@usp.br
‡Product Development Engineer, Embraer, São José dos Campos, Brazil. leandro.simoes@embraer.com.br
§USP, SEA, São Carlos, Brazil. marcello@sc.usp.br

I. Introduction

In the last few decades, aircraft engines have undergone many advances in noise reduction, such as use of high by-pass turbofans, acoustic liners and noise suppression nozzle shapes. This fact summed to the low thrust applied on engines during the landing phase brings the airframe noise as one of the most important noise sources during this flight phase.[1] Among the airframe noise sources, the most important components are the landing gear, flap side edges and the slat. The importance of the slat as noise source is highlighted by the fact that it is distributed along almost the whole wing span.

A number of experiments carried out to study slat noise generation and radiation were published,[1–4] making it possible to separate the slat noise into three main components. One of them is a high frequency tone, another one is a broadband noise at low and medium frequencies and finally the third component of slat noise is comprised of tonal peaks superposing the low-medium frequency broadband noise. Both experimental[2,3] and numerical[5,6] works studied the tonal high-frequency peak and its generation is attributed to the vortex shedding at the slat trailing edge. However, this noise component is found only on models,[1] given the constructive restrictions to build trailing edges as thin as the scaled model would require. Experiments[7,8] have actualy shown that the broadband spectrum is the only noise component found in full-scale models, attributing the multiple tonal peaks to the low Reynolds number of wind-tunnel experiments. Their generation is not yet fully understood but some theories based on Rossiter[9] or Parker[1] modes are proposed.

Along with the above experiments, 2D simulations were initially carried out,[10–13] aiming at better understanding the unsteady behavior of the flow in the slat cove region. Two companion works[3,13] used PIV images to assess the accuracy of unsteady flow solutions produced by 2D computational simulation. The computational averaged velocity field compared well with experiments but the numerical calculation resulted in substantialy larger spanwise votices in slat cove than the vortices observed in PIV images. The use of a three-dimensional domain with an extruded airfoil[14,15] achieved better agreement with PIV measurements for the instantaneous spanwise vorticity field in the slat cove. This indicated the need to consider three-dimensional phenomena to proper simulate the flow structures in the slat cove. Time-accurate 3D simulations were carried out using the Lattice-Boltzmann formulation and compared with results based on Navier-Stokes calculations. Good agreement in the instantaneous spanwise vorticity field was achieved as well as in near-field fluctuations spectra.[16] Based on the observation that different slat boundary layer solutions did not produce significant change in the generated sound, a model considering free-slip boundary condition on the slat surface was proposed.[17] This approach allows cheaper simulations, since the restiction of a maximum value for y^+ close to the wall does not apply to frictionless walls.

Most of the simulations aiming at studying the flow around the slat and its noise consider idealized clean geometries. Nevertheless the slats installed in actual airplanes possess several small elements in the cove region. Such geometrical details include slat deflection mechanisms, anti-icing tubes, and seals (Fig. 1). These elements can change the flow dynamics and therefore the characteristics of the propagated noise. 2D simulations were carried out to assess the effect of different blade seal configurations on the slat noise,[18] showing that an extended seal at the slat cusp reduces the amplitude of the radiated sound. Other element included in the geometry of those simulations[18] was the bulb seal that prevents the metal-metal friction between the slat lower surface and the main element upper surface and seals the space between the two elements in cruise configuration. However, no difference was observed in the noise signature between the configurations with and without the bulb seal, and is generally regarded as harmless. The work described here analyses the consequences to the slat unsteady flow field and noise generation of a bulb seal of various heights located at various points in the slat cove. It is find that the bulb seal can have a very detrimental effect on the slat noise performance.

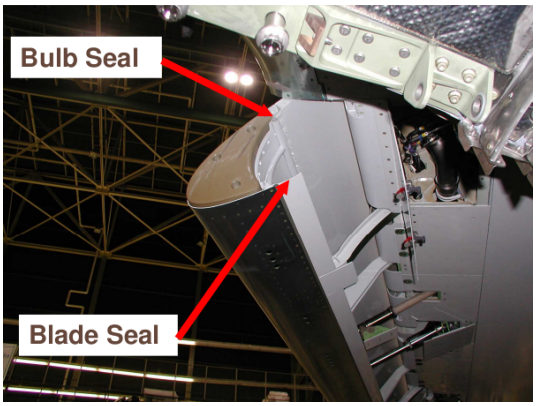

Figure 1. Photo of the slat cove of a Boeing 777. From Khorrami and Lockard (2006).[18]

II. Simulated Geometry

The present simulations used the 30P30N airfoil as basic geometry. This is a high-lift airfoil extensively studied by NASA, both aerodynamically[19] as well as aeroacoustically.[3,11,14,20,21] Some characteristics of the 30P30N airfoil are presented in table 1. The slat and flap chords are 15% and 30% of the airfoil stowed chord, respectively. In the simulations, only the slat trailing edge had a finite thickness of $0.42mm$. However the computational mesh was not refined enough in the trailing edge region to capture the slat vortex shedding.

Table 1. 30P30N geometry parameters

	Deflection	Gap	Overhang
Slat	30°	2.95%	-2.95%
Flap	30°	1.27%	0.25%

A modification was made on the slat cove surface of the 30P30N geometry to consider the presence of the seal (Fig. 2 and 3). The variations in the position and height of the device are described in table 2. The distance s corresponds to the distance between the device and the slat trailing edge along the curved surface. The values are normalized by the distance between the reattachment point and the trailing edge ($s_{rp} = 6.8mm$). On the other hand, the height h is normalized by the slat trailing edge thickness (δ_{TE}). The seal width was kept constant and equal to three times the slat trailing edge thickness in all simulations.

Table 2. Description of simulated cases.

	s/s_{rp}	h/δ_{TE}
Case 1	2	3
Case 2	2	6
Case 3	2	12
Case 4	3	6
Case 5	1	6

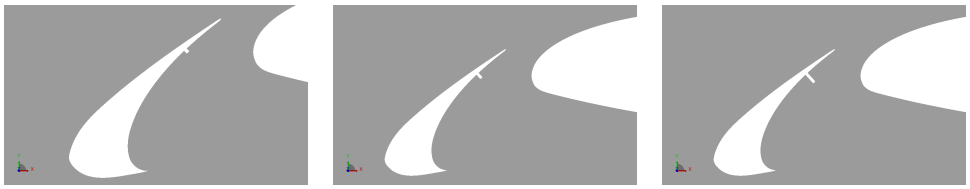

(a) Case 1 (b) Case 2 (c) Case 3

Figure 2. Simulated geometries with different seal heights.

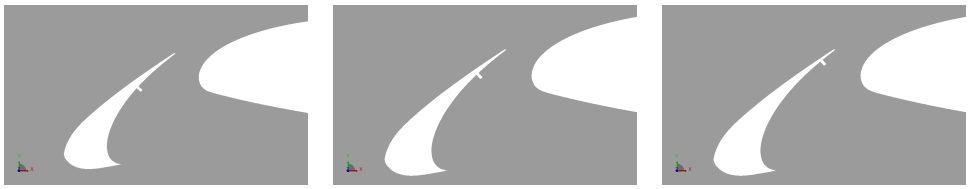

(a) Case 4 (b) Case 2 (c) Case 5

Figure 3. Simulated geometries with different seal positions.

III. Numerical Model

The simulations described in this paper used the commercial code PowerFLOW 4.3a, by EXA. It is based on the lattice-Boltzmann method that solves the discrete Boltzmann equation for the probability density function f using a Bhatnagar, Gross and Krook (BGK)[22] approximation for the colision term,

$$f(\vec{r}+\vec{c}\delta t,\vec{c},t+\delta t)-f(\vec{r},\vec{c},t)=-\frac{1}{\tau}\left[f(\vec{r},\vec{c},t)-f^{eq}(\vec{r},\vec{c},t)\right]. \quad (1)$$

To calculate the effect of subgrid turbulent scales, a turbulence model based on the $k-\epsilon$ RNG is employed. The program uses a cartesian mesh to discretize the domain and a volumetric form of the equation 1 is solved to enable the solution of problems with complex geometries.[23] The calculation of the sound propagated to the far-filed is made by means of a Ffowcs Williams-Hawkings analogy algorithm.[24] The surface of integration of the Ffowcs Williams-Hawkings method coincided with the slat surface.

The simulation model was scaled to match the experiments from Jenkins et al.,[3] resulting in a Reynolds number of 1.7 million based on the stowed chord $c = 0.457m$ and free stream velocity $U_\infty = 56m/s$, with a Mach number of $M = 0.17$. The wind tunnel blockage effect was also taken into account by placing free-slip walls according to the tunnel dimensions.[3] The simulated span was equal to $0.5078m$. Periodicity was adopted in the boundary planes normal to the spanwise direction, which corresponds to the assumption of homogeneity in this direction. The angle of attack used in all simulations was $4°$.

Once the flow conditions and the airfoil angle of attack simulated in the present work were the same as the conditions simulated by Simões et al.,[17] the free-slip wall condition was adopted to represent the slat surface, except at the cove wall. Therefore, the less demanding grid topology called "optimized mesh" in this reference[17] was used. Figure 4 shows the detail of the mesh in the slat region.

Based on the grid independence study made by Simões et al.,[17] all configurations described in the present work were simulated using a mesh that had its smallest element of $0.2mm$ in the region of slat cove and flap leading edge. This mesh had a total of approximately 1.04×10^8 voxels. Additionally, case 1 was simulated using a mesh with finest voxels of $0.15mm$. The same grid topology were used and the regions of coarser elements were refined proportionally. In this case because of mesh refinement, the domain dimension in spanwise direction were proportionally reduced.

All simulations were made to have a physical time sample of $0.25s$. Analysis of time averaged values and autocorrelation spectra indicated that discarding the initial $0.1s$ of the simulations were enough to achieve statistical convergence of the data. So the time samples used to calculate mean and spectral values range from $0.1s$ to $0.25s$ in all cases analysed in this work.

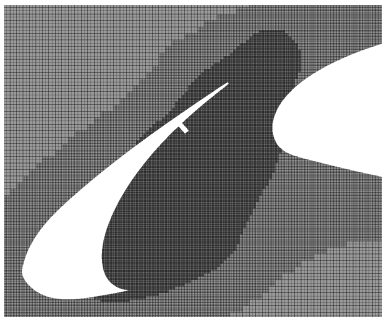

Figure 4. Grid configuration in slat cove region.

IV. Results

IV.A. Effect of Seal Height

To evaluate the effect of the seal height, three configurations of seal were analysed and compared with the clean airfoil and with each other. In the three cases with the seal it was positioned at a distance from the trailing edge that is twice the distance between the reattachment point and the trailing edge. The cases with the seal discussed in this section are cases 1, 2 and 3 in table 2.

The time averaged C_p distributions of these three configurations with the seal as well as for the clean airfoil are compared in figure 5(a) and the detail of the slat is given in figure 5(b). The distribution refers to the central section of the simulated span. Significant variation in static pressure distribution occurs only in the region next to the seal, but these alterations does not cause a variation in the overall airfoil's pressure distribution.

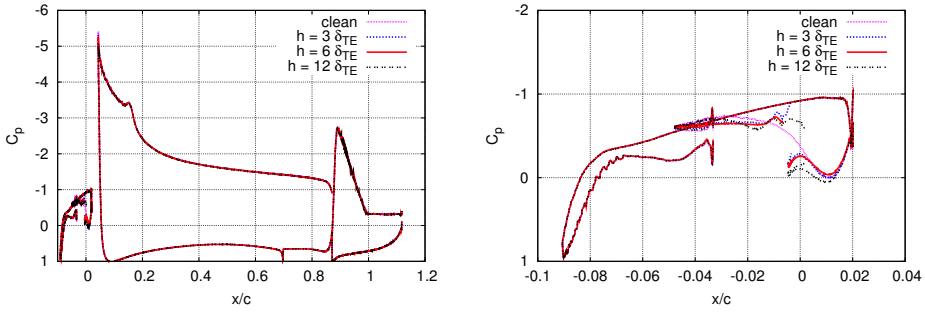

(a) Airfoil (b) Slat

Figure 5. Pressure coefficient distribution (a)along airfoil surface and, in detail, (b)along the slat surface. Comparison between three different seal sizes and clean configuration.

Figure 6 shows the time-averaged streamlines in the central section of slat cove region. Although the size of the seal suffered a considerable variation between the cases, no significant change is observed in the averaged flow pattern. As the mixing layer reattaches, part of the flow is pumped through the slat gap and part of it is directed towards the seal, streams over it and is trapped inside the cove. An interesting effect that is observed in the $h = 3\delta_{TE}$ and $h = 6\delta_{TE}$ is the translation of the center of recirculation relative to the clean configuration. This translation is not so clear in the case with $h = 12\delta_{TE}$

The non-dimensional Turbulent Kinetic Energy (TKE), calculated by $0.5(\langle u'u'\rangle + \langle v'v'\rangle + \langle w'w'\rangle)/U_\infty^2$, in the central section is showed in figure 7 for the three different sizes of seal and the clean slat. It is clear that the presence of the seal reduces substatially the intensity of the fluctuations inside the recirculation zone, mainly in the cases with $h = 3\delta_{TE}$ and $h = 6\delta_{TE}$. It is seen also that these two cases have a bigger region of intense TKE next to the reattachment point than the other two cases. This is related to the variation of the recirculation center, since the vortical structures inside the cove recirculate closer to the reattachment region in these cases.

The variable λ_2 is used to identify vortex core in figure 8. Isosurfaces of $\lambda_2 = -10000$ are ploted inside

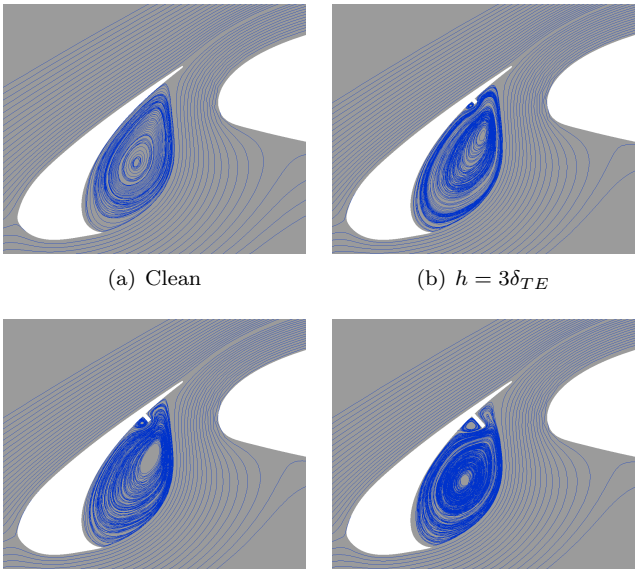

(a) Clean (b) $h = 3\delta_{TE}$

(c) $h = 6\delta_{TE}$ (d) $h = 12\delta_{TE}$

Figure 6. Time averaged streamlines in cove region for geometries with three seal sizes and clean configuration.

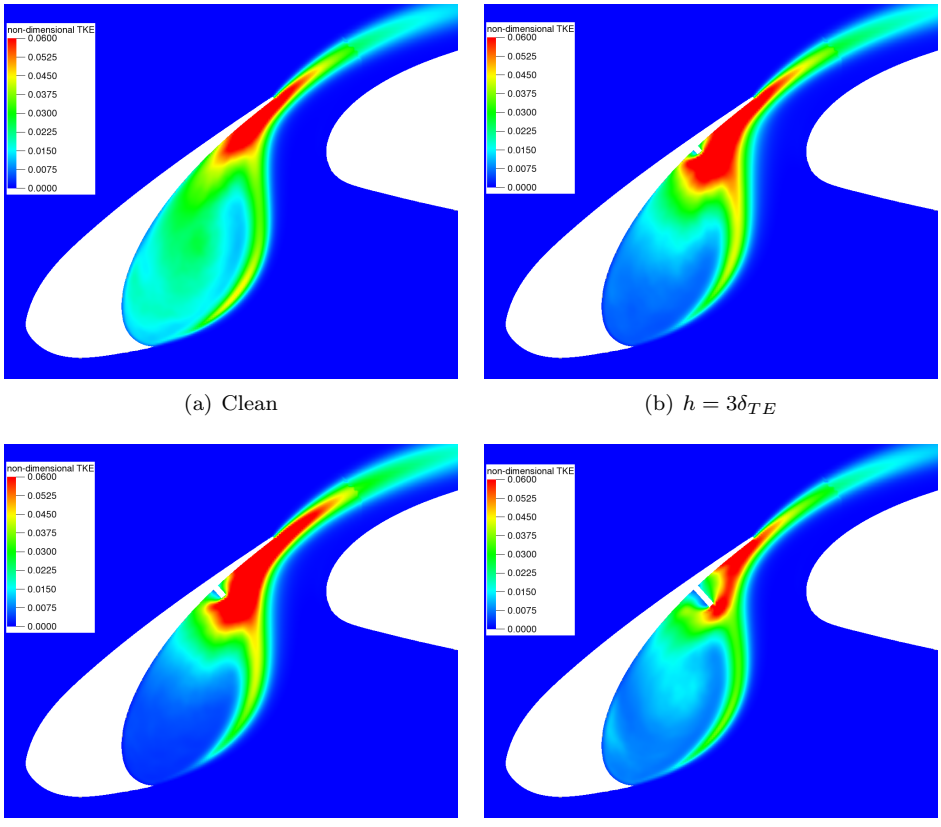

(a) Clean (b) $h = 3\delta_{TE}$

(c) $h = 6\delta_{TE}$ (d) $h = 12\delta_{TE}$

Figure 7. Turbulent kinetic energy field in the slat cove with different seal sizes.

the cove region. As indicated by the TKE contours, the isosurfaces of λ_2 also show less structures inside the cove in cases $h = 3\delta_{TE}$ and $h = 6\delta_{TE}$. It is also clear that the vortices formed in the mixing layer are much more bi-dimensional in the three cases with the seal. This observation is in accordance with the statement that the structures inside the recirculation zone are responsible to initiate three-dimensionalization of the mixing layer vortices.[14]

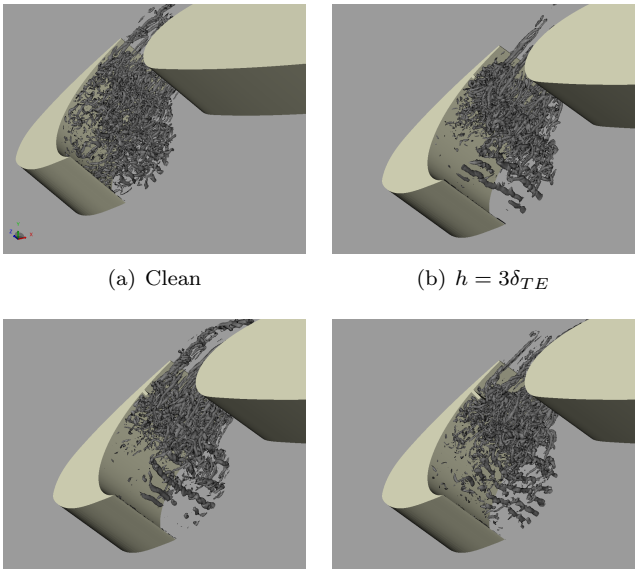

(a) Clean (b) $h = 3\delta_{TE}$

(c) $h = 6\delta_{TE}$ (d) $h = 12\delta_{TE}$

Figure 8. Isosurfaces of negative λ_2 showing the vortical structures inside the slat cove with different seal sizes.

The effect of the seal can be perceived also in the spectral distribution of fluctuations of streamwise velocity component (u') in the mixing layer next to the cusp. The figure 10(d) compares the Power Spectral Desity of u' in the position $S/S_{max} = 0.20$, according to the nomeclature presented in figure 9.[20] Strouhal number is based on the slat chord (c_s) and inlet velocity (U_∞). Comparing the spectra of the cases with seal against the clean geometry, it is seen that the seal causes the reduction of broadband fluctuations next to the cusp and this effect is more pronounced in the two cases with smaller seals ($3\delta_{TE}$ and $6\delta_{TE}$). Nevertheless the tonal peaks between $St = 1$ and $St = 6$ are enforced with the presence of the seal in these cases. Analysing the fluctuations of u' along the mixing layer towards the reattachment location it can be seen that the intensity of broadband fluctuations of the cases with seal approaches gradually the intensity of the clean geometry. Indeed at the point closest to the reattachment ($S/S_{max} = 0.81$) the only difference between the spectrum of the cases with seal and the one without it is the level of the tonal peaks.

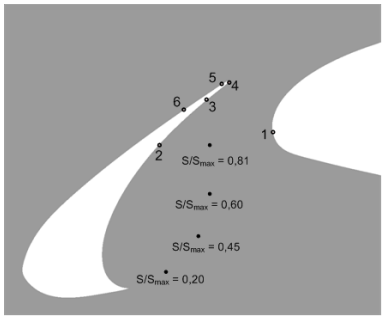

Figure 9. Near-field points where Power Spectral Density were calculated.

Figure 11 compares spectra of the noise propagated to the far-field from the slat region of the four cases considered in this section. The integration using Ffowcs Williams-Hawkings analogy was carried out relative to a point at a distance from the slat cove equal to ten times the chord of the airfoil in stowed configuration

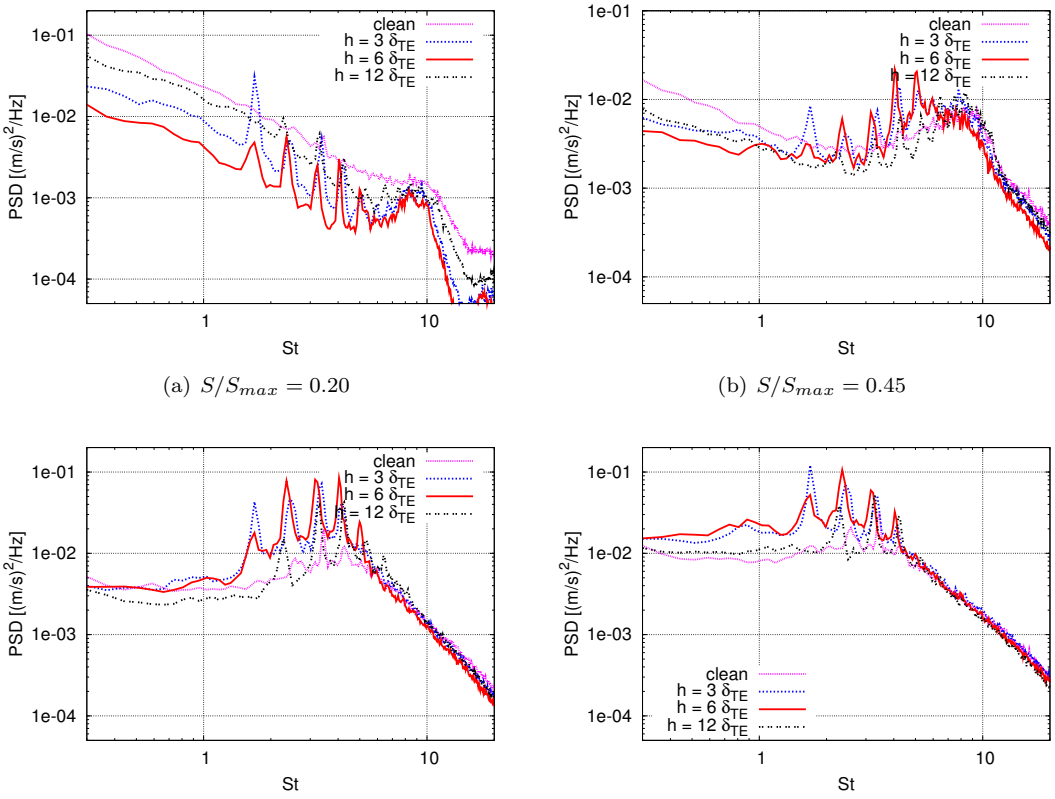

(a) $S/S_{max} = 0.20$

(b) $S/S_{max} = 0.45$

(c) $S/S_{max} = 0.60$

(d) $S/S_{max} = 0.81$

Figure 10. Spectra of u' along the slat mixing layer comparing the clean configuration and the three geometries with different seal sizes.

at a polar angle of 290°, where 0° corresponds to a point downstream from the airfoil. Significant differences between the cases are observed only at frequencies under $St = 4$. The basic effect of the seal in the noise propagated by the slat is the intensification of the tonal peaks at lower frequencies by up to $14dB/Hz$. Nonetheless the biggest seal tested do not cause a significant increase in the level of the peaks as the other two seal geometries.

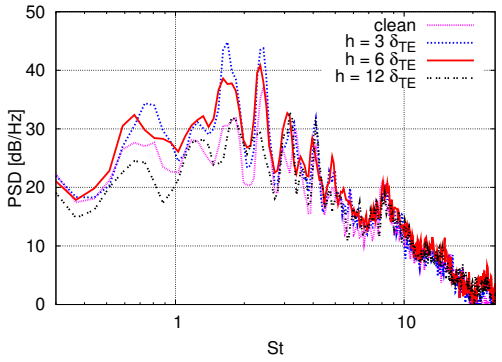

Figure 11. Comparison of spectra of far-field pressure fluctuations at 290°. Different seal sizes.

IV.B. Effect of Seal Position

Using the seal of height equal to 6 times the trailing edge thickness, three position were compared against each other as well as with the clean configuration. In the discussions of this section, the cases regarded as $s = 2s_{rp}$ is the same as case $h = 6\delta_{TE}$ of last section. From figure 12, it can be seen that the seal, at the three positions tested, have no significant effect on the general pressure distribution over the airfoil surface pressure. The variations observed are concentrated in the region next to the seal.

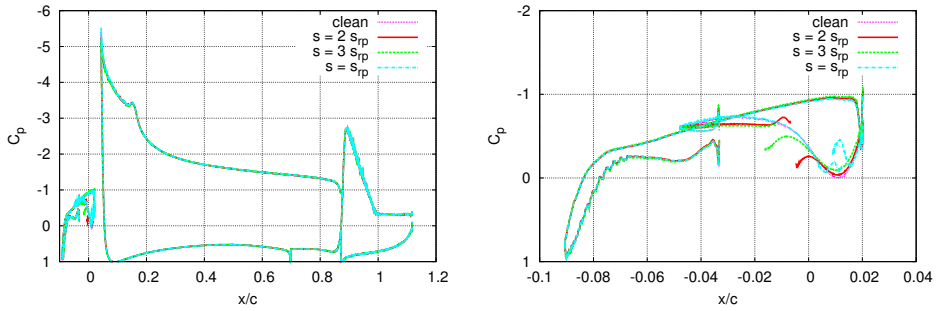

(a) Airfoil (b) Slat

Figure 12. Pressure coefficient distribution along airfoil surface and, in detail, along the slat surface. Comparison between three different seal positions and the clean configuration.

The time averaged streamlines presented in figure 13(d) show that, as happens to the geometries with the seal located at $s = 2s_{rp}$, the seal at the reattachment point also do not cause significant modification on the mean flow pattern in the slat cove. Positioning the seal farther from the trailing edge on the other hand can change radically the flow in this region as shown in figure 13(b). In this case the recirculation zone is divided in two counter-rotating flow regions of comparable size.

The contours of TKE in the cove region presented in figure 14 show that in case 4 the cove flow has bigger region of intense fluctuations, starting next to the cusp and ranging almost the entire outside recirculation zone. The inside recirculating zone on the other hand present much less turbulent kinetic energy as the seal works as a barrier to the vortical structures that keep traped and recirculating predominantely in the outside zone, as can be seen in the instantaneous field of spanwise vorticity component (Fig. 15). From figure 14 it can be seen also that, positioned at the reattachment point, the seal do not block the vortices from the

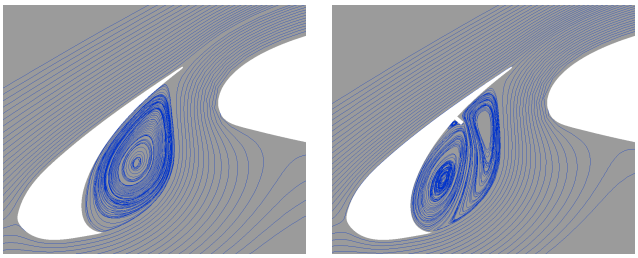

(a) Clean (b) $s = 3s_{rp}$

(c) $s = 2s_{rp}$ (d) $s = s_{rp}$

Figure 13. Time averaged streamlines in cove region for geometries with three seal positions and the clean configuration.

mixing layer and the TKE in the cove in this case is comparable to the TKE in clean configuration. Also the unsteady flow dynamic of the two cases is very similar (Fig. 15).

Figure 16 compares spectra of u' in four points of the mixing layer showed in figure 9. As was expected from the contours of TKE, in points closer to the cusp, the levels of the spectra from case 4 are the highest in general. Although the spectra from this case become gradually more similar to the other cases as one approches the reatachment point, at $S/S_{max} = 0.81$ some differences are still perceived, e.g. the maximum PSD displaced to lower frequencies. The spectra of u' also confirms the similarity between the flow around the clean geometry and the slat with the seal located at the reattachment location, since in the four points analysed, the spectra of both cases are practically identical.

Spectra of pressure fluctuations in three points at slat surface are presented in figure 17. Since the seal of case 4 is placed over point 2, this case is not represented in figure 17(a). For the same reason case 5 is not represented in figure 17(b). The spectrum of surface pressure fluctuations further indicates the similarity between the clean configuration and the configuration with the seal at reattachment point. In point 2, the spectra of theses cases are practically equal and, in point 6, they present differences in the position and intensity of the peaks but have similar broadband noise levels. Inside the recirculation region (point 2), the geometry with the seal at $s = 2s_{rp}$ has a lower level of fluctuations in higher frequencies compared to the other two cases showed in figure 17(a). This can be due to the blockage effect that the seal has over the vortices formed in the mixing layer and directed to the recirculation zone after impinging the cove wall. In point 6, where most of the fluctuations are consequence of acoustic waves, the cases with the seal in the recirculation zone present stronger peaks in lower frequencies band.

The spectra of the noise propagated from the slat to the far-field are presented in figure 18 for the four cases compared in this section. The point considered in the Ffowcs Williams-Hawkings calculations is the same as in figure 11, i.e. at a distance from the slat cove of ten airfoil chords in stowed configuration and a polar angle of 290°. As consequence of the similar flow characteristics between the clean geometry and the slat with seal at reattachment point, the noise produced by these two configurations are almost the same, with some difference in the level of the peak at $St \approx 1.7$. The other two configurations, namely the ones with the seal inside the recirculation zone, have higher noise levels at frequencies under $St = 3$. Additionally the noise spectrum of the $s = 3s_{rp}$ configuration present two peaks below $St = 2$ which are not similar to the peaks in any other configuration, probably because of the odd characteristics of the cove flow pattern in this case. The difference between the PSD of the geometry with seal at $s = 3s_{rp}$ and the PSD of the clean geometry is as big as $15dB/Hz$ at $St = 0.8$.

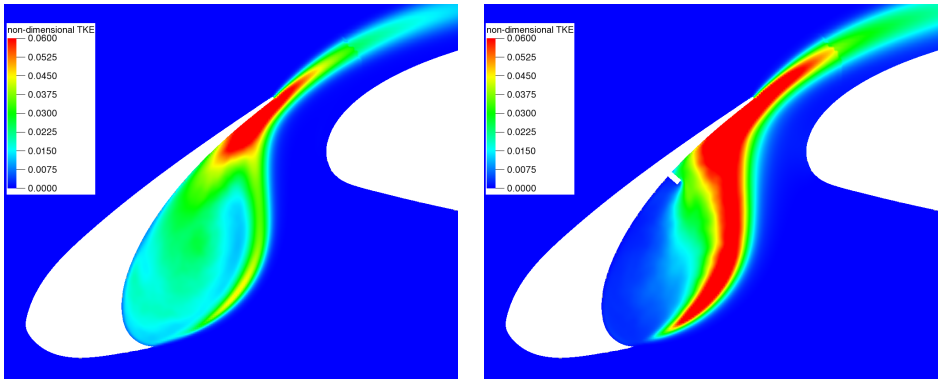

(a) Clean (b) $s = 3s_{rp}$

(c) $s = 2s_{rp}$ (d) $s = s_{rp}$

Figure 14. Turbulent kinetic energy field in the slat cove with different seal positions.

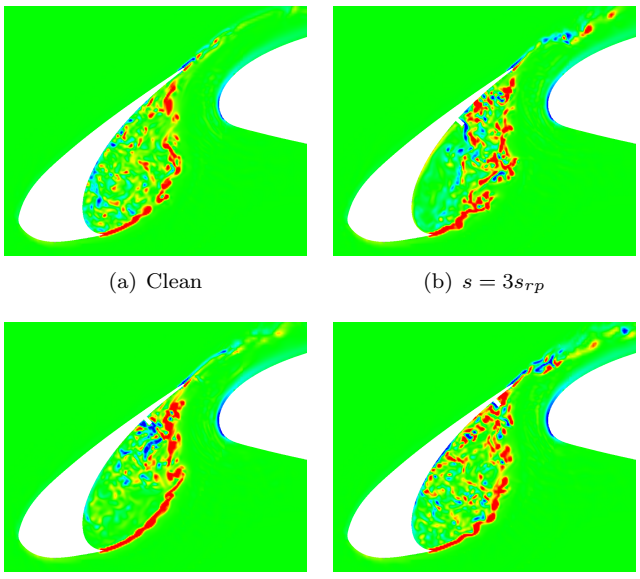

(a) Clean (b) $s = 3s_{rp}$

(c) $s = 2s_{rp}$ (d) $s = s_{rp}$

Figure 15. Snapshot of spanwise vorticity component for three different seal positions as well as for the clean configuration.

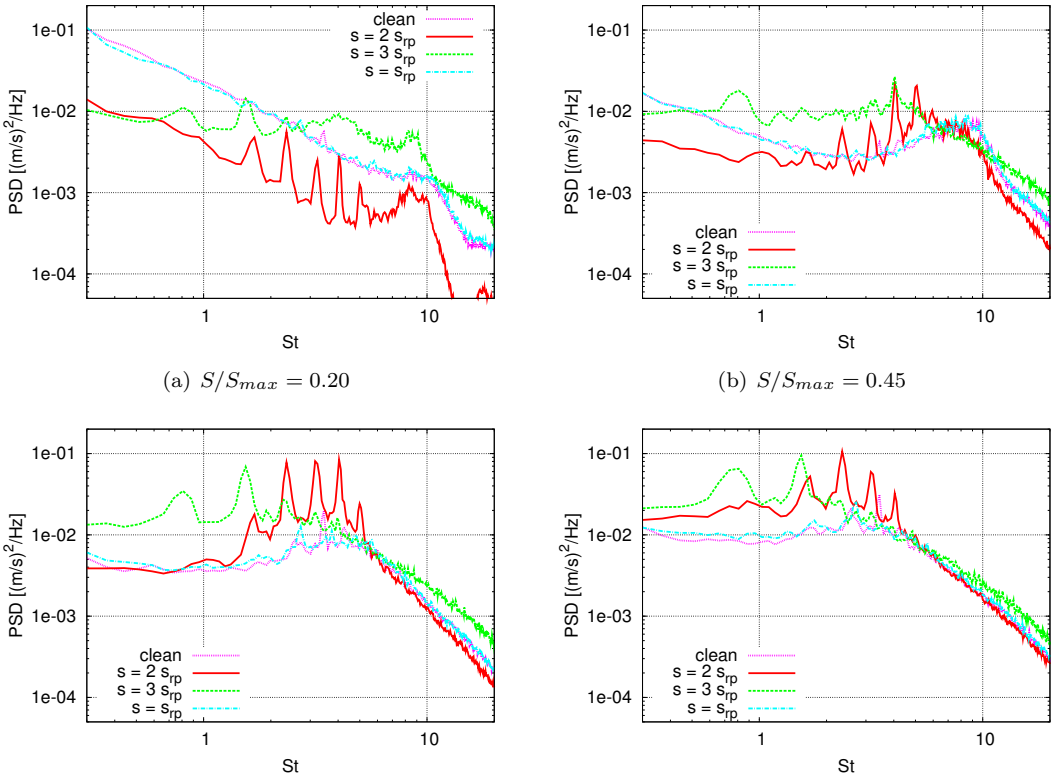

(a) $S/S_{max} = 0.20$

(b) $S/S_{max} = 0.45$

(c) $S/S_{max} = 0.60$

(d) $S/S_{max} = 0.81$

Figure 16. Spectra of u' along the slat mixing layer comparing the clean configuration and the three geometries with different seal positions.

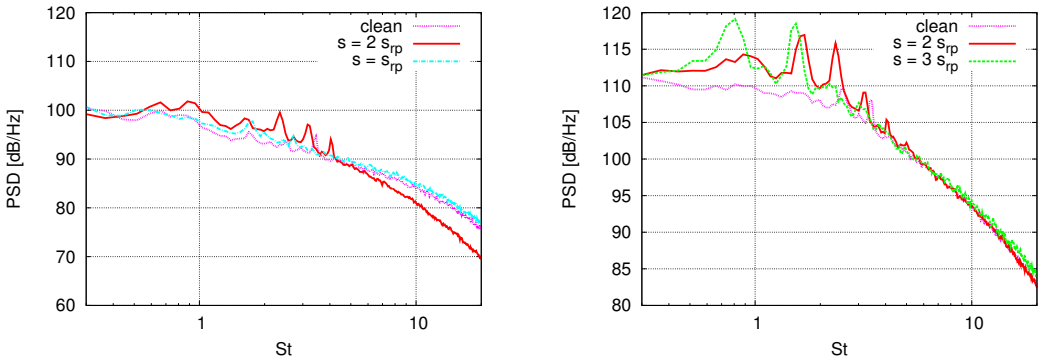

(a) Point 2

(b) Point 3

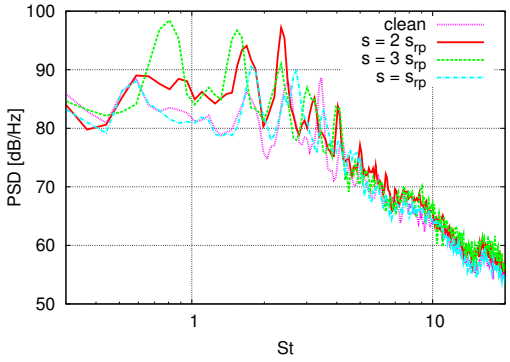

(c) Point 6

Figure 17. Spectra of u' along the slat mixing layer comparing the clean configuration and the three geometries with different seal positions.

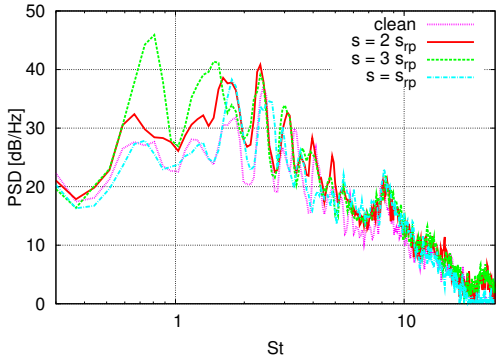

Figure 18. Comparison of spectra of far-field pressure fluctuations at 290°. Three seal positions.

IV.C. Grid Independence Study

Two simulations with the geometry with the seal located at $s = 2s_{rp}$ and $3\delta_{TE}$ high were carried out using different grid refinement. The designations $\delta x_{min} = 0.20mm$ and $\delta x_{min} = 0.15mm$ refers to size of the edge of the smallest voxel. Figure 19 presents the time averaged pressure coefficient distribution on the the central section of overall airfoil and the detail of the distribution on the slat. The grid refinement causes no significant change in the airfoil pressure distribution.

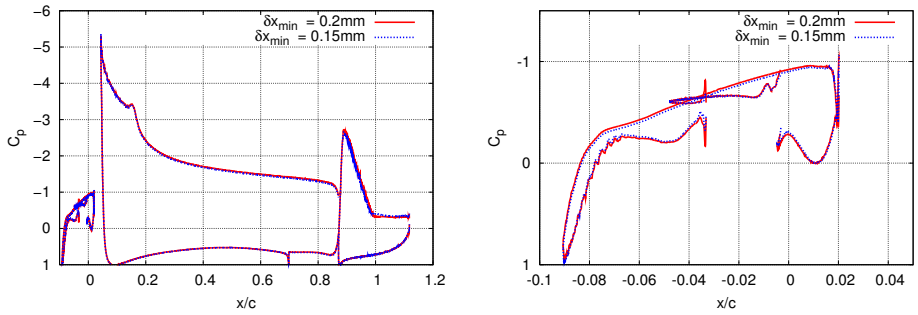

(a) Airfoil (b) Case 2

Figure 19. Pressure coefficient distribution along airfoil surface and, in detail, along the slat surface.

The Turbulent Kinetic Energy calculated by the two grid refinements are compared in figure 20. It also indicates a convergence of the mean solution respective to the grid resolution. Nevertheless a small difference between the solutions can be observed in the development of the disturbances half way along the mixing layer. In the solution with the finest mesh (Fig. 20(b)), a narrow region with TKE slightly higher than its neighborhood can be observed. Such a behavior is not seen in the contour of the coarser mesh. This difference can be also observed in the spectrum of fluctuations of the streamwise velocity component in the point $S/S_{max} = 0.20$ showed in figure 21(a). The comparison of the spectra in this figure show an increase in the frequency of the broad peak around $St = 10$. This peak is probably related to the amplification of disturbances in the unstable mixing layer. Figure 24 show the velocity profile along the black line displayed in figure 20(b). As can be seen, the calculation with finer mesh results in a narrower mixing layer. So in this point, the the most amplified frequency is highr than the one of the simulation with coarse grid.

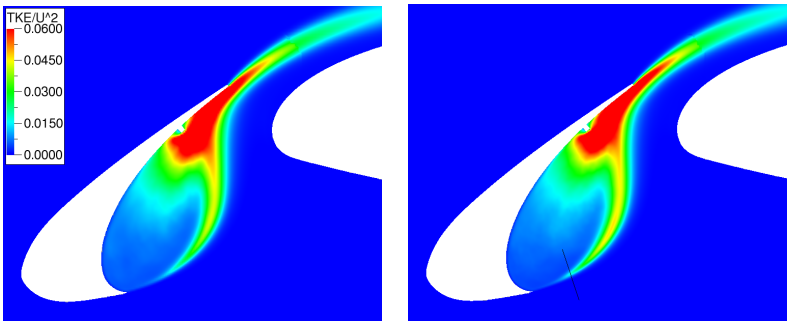

(a) $\delta x_{min} = 0.20mm$ (b) $\delta x_{min} = 0.15mm$

Figure 20. TKE contours in cove region for the two mesh refinement configurations.

The PSD of pressure fluctuations at the points of the airfoil surface showed in figure 9 were also calculated. The spectra of three of these points are showed in figure 23. In the slat trailing edge (point 4) the refinement of the mesh causes a substantial modification in the spectrum. Several experiments and wind tunnel experiments have shown the process of vortex shedding from the slat trailing edge. Although none of the two meshes is fine enough to solve this shedding of vortices, the finer one can solve fluctuations of higher frequencies. The same shift of the fluctuations around $St = 10$ seen in spectrum of point $S/S_{max} = 0.20$ is observed in surface point 6. As this point is located outside the slat cove, this suggests that the fluctuations at this frequency band in the mixing layer are propagated as sound waves. Despite the significant variation

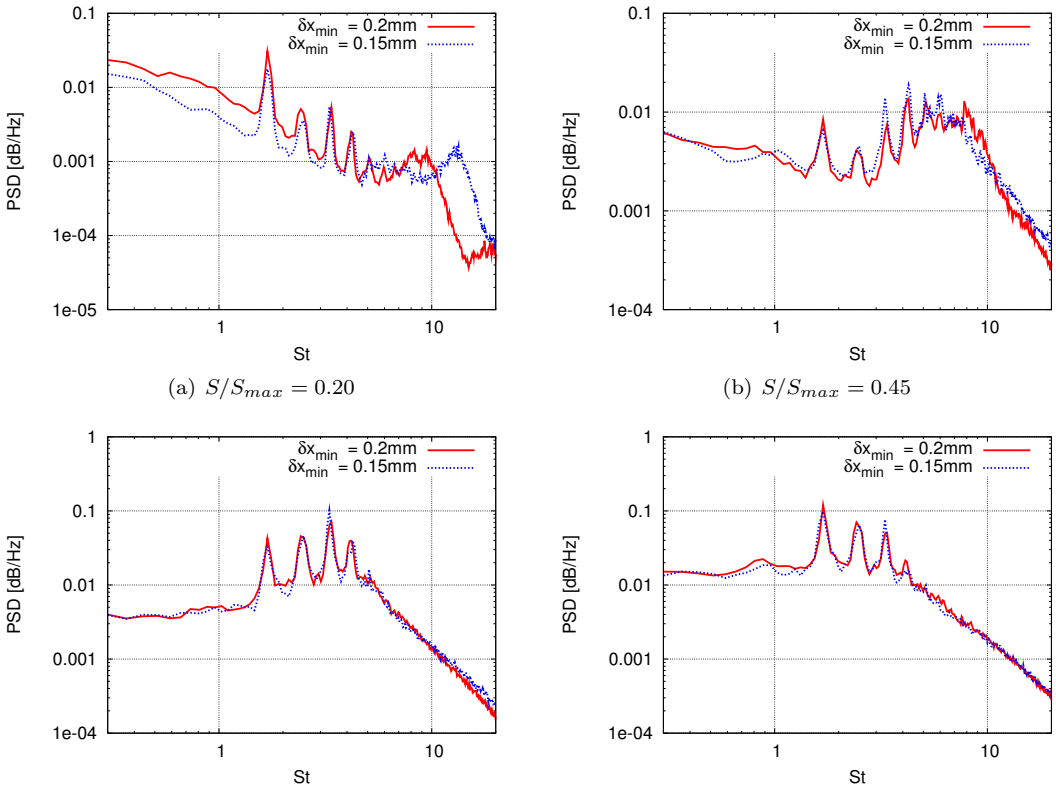

(a) $S/S_{max} = 0.20$ (b) $S/S_{max} = 0.45$

(c) $S/S_{max} = 0.60$ (d) $S/S_{max} = 0.81$

Figure 21. Power Spectral Density of the fluctuations of streamwise velocity component.

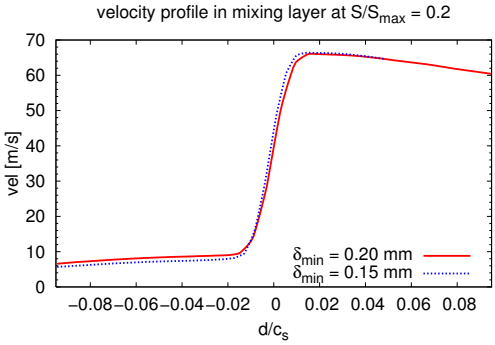

Figure 22. Velocity profile across the mixing layer at position $S/S_{max} = 0.20mm$.

of the spectra in point 4 and 6, the outher analysed points present similar PSD curves regardless of which of the two tested grid were employed, so that the graphics of points 1, 2 and 5 present as good comparison between the meshes as the spectrum in point 3.

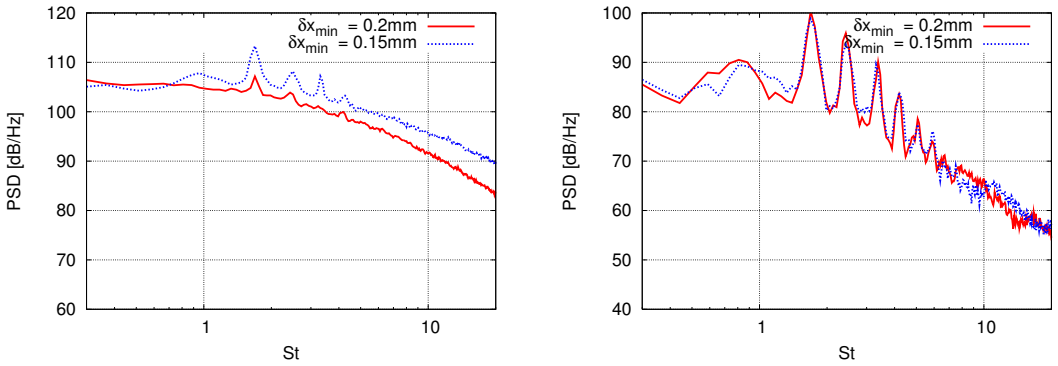

(a) Point 4 (b) Point 6

Figure 23. Power Spectral Density of the fluctuations of static pressure on two points of the slat surface.

The frequency shift observed in the mixing layer fluctuations can be perceived also in the far-field as shows the spectrum in figure 24, calculated with the time history of a Ffowcs Williams-Hawkings integration for a point at a distance of ten airfoil stowed chords from the slat cove. This means that this frequency band of the spectrum needs even finer resolution of the spatial discretization to be calculated and further mesh refinement is required to garantee independence of the solution. Nevertheless this observation indicates the efficiency as sound source of the turbulence occurring in the mixing layer mid way from the cusp to the reattachment point.

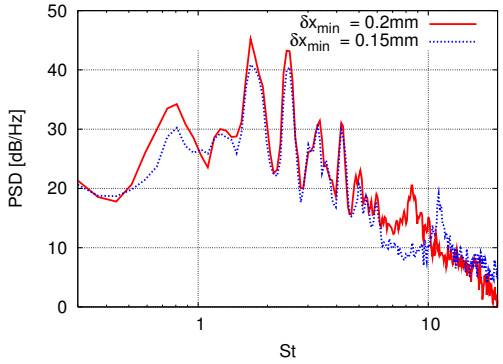

Figure 24. Power Spectral Density of the pressure fluctuations in the far-field at 290°.

V. Conclusion

Numerical simulations were carried out to assess the effect of a excrescence on the noise generated by the slat. The simulated geometries were based on the high-lift airfoil MD 30P30N and the included element resembled a seal located at the slat cove surface. The effect of both height and position of the seal was analysed. The effect of seal in the pressure distribution was minimal regardless of the height and location of the seal. Positioned between the cusp and the reattachment point, the seal works as a barrier to the vortices formed in the mixing layer and reduces the intensity of fluctuations inside the cove. As a consequence, the level of some tonal peaks of low frequencies are increased in the far-field noise spectrum. Simulation with a finer mesh showed that fluctuations of a specific frequency band inside the mixing layer are still grid dependent and further simulations are needed to ensure model convergence. Since similar variations of the spectrum were observed in the near-field and far-field fluctuations, it indicates the importance in noise

generation of mixing layer turbulence far from the reattachment point.

References

[1]Dobrzynski, W., "Almost 40 Years of Airframe Noise Research: What Did We Achieve?", Journal of Aircraft, Vol. 47, No. 2, March-April 2010.

[2]Choudhari, M. M., Lockard, D. P., Macaraeg, M. G., Singer, B. A., Streett, C. L., Neubert, G. R., Stoker, R. W., Underbrink, J. R., Berkman, M. E., Khorrami, M. R., Sadowski, S. S., "Aeroacoustic Experiments in the Langley Low-Turbulence Pressure Tunnel", NASA TM-2002-211432, February 2002.

[3]Jenkins, L. N.,Khorrami, M. R., Choudhari, M., "Characterization of Unsteady Flow Structures Near Leading-Edge Slat: Part I. PIV Measurements", AIAA Paper 2004-2801, 2004.

[4]Imamura, T., Ura, H., Yokokawa, Y., Yamamoto, K., "A Far-field Noise and Near-field Unsteadiness of a Simplified High-Lift-configuration Model (Slat)", AIAA Paper 2009-1239, 2009.

[5]Khorrami, M. R., Berkman, M. E., Choudhari, M. M., "Unsteady Flow Computations of a Slat With a Blunt Trailing Edge", AIAA Journal, Vol. 38, No. 7, 2000.

[6]Singer, B. A., Lockard, D. P., Brentner, K. S., "Computational Aeroacoustic Analysis of Slat Trailing Edge Flow", AIAA Journal, Vol. 38, No. 9, 2000.

[7]Dobrzynski, W., Nagakura, K., Gehlhar, B., Buschbaum, A., "Airframe Noise Studies on Wings with Deployed High-Lift Devices", AIAA Paper 1998-2337, 1998.

[8]Dobrzynski, W., Pott-Pollenske, M., "Slat Noise Source Studies for Farfield Noise Prediction", AIAA Paper 2001-2158, 2001.

[9]Kolb, A., Faulhaber, P., Drobietz, R., Grnewald, M., "Aeroacoustic Wind Tunnel Measurements on a 2D High-Lift Configuration", AIAA Paper 2007-3447, 2007.

[10]Khorrami, M. R., Singer, B. A., Berkman, M. E., "Time-Accurate Simulations and Acoustic Analysis of Slat Free-Shear-Layer", AIAA Journal, Vol. 40, No. 7, July 2002, pp. 1284-1291.

[11]Khorrami, M. R., Singer, B., Lockard, D., "Time-Accurate Simulations and Acoustic Analysis of Slat Free-Shear-Layer: Part II", AIAA Paper 2002-2579, 2002.

[12]Choudhari, M. M., Khorrami, M. R., Lockard, D. P., Atkins, H. L., Lilley, G. M., "Slat Cove Noise Modeling: A Posteriori Analysis of Unsteady RANS Simulations", AIAA Paper 2002-2468, 2002.

[13]Khorrami, M. R., Choudhari, M., Jenkins, L. N., "Characterization of Unsteady Flow Structures Near Leading-Edge Slat: Part II. 2D Computations", AIAA Paper 2004-2802, 2004.

[14]Choudhari, M. M., Khorrami, M. R., "Effect of Three-Dimensional Shear-Layer Structures on Slat Cove Unsteadiness", AIAA Journal, Vol. 45, No. 9, September 2007.

[15]Imamura, T., Enomoto, S., Yamamoto, K., "3D Unsteady Flow Computations in a Slat Cove Using Large Eddy Simulation", AIAA Paper 2006-2668, 2006.

[16]Aflalo, B. S., Simões, L. G. C., Silva, R. G., Medeiros, M. A. F., "Comparative Analysis of Turbulence Models for Slat Noise Source Calculations Employing Unstructured Meshes", AIAA Paper 2010-3838, 2010.

[17]Simões, L.G.C., Souza, D. S., Medeiros, M. A. F., "On the Small Effect of Boundary Layer Thicknesses on Slat Noise", AIAA Paper 2011-2906, 2011.

[18]Khorrami, M. R., Lockard, D. P., "Effects of Geometric Details on Slat Noise Generation and Propagation", AIAA Paper 2006-2664, 2006.

[19]Klausmeyer, S. M., Lin, J. C., "Comparative Results From a CFD Challenge Over a 2D Three-Element High-Lift Airfoil", NASA Technical Memorandum 112858, May 1997.

[20]Lockard, D. P., Choudhari, M. M., "Noise Radiation from a Leading-Edge Slat", AIAA Paper 2009-3101, 2009.

[21]Lockard, D. P., Choudhari, M. M., "The Effect of Cross Flow on Slat Noise", AIAA Paper 2010-3835, 2010.

[22]Bhatnagar, P. L., Gross, E. P., Krook, M., "A Model for Colision Processes in Gases. I. Small Amplitude Processes in Charged and Neutral One-Component System", Physical Review, Vol. 94, No. 3, 1954, pp. 511-525.

[23]Chen, H., Teixeira, C., Molvig, K., "Realization of Fluid Boundary Conditions via Discrete Boltzmann Dynamics", International Journal of Modern Physics C , Vol. 10, 1999.

[24]Brès, G. A., Pérot, F., Freed, D., "A Ffowcs Williams-Hawkings Solver for Lattice-Boltzmann based Computational Aeroacoustics", AIAA Paper 2010-3711, 2010.